JTTEE5 12:95-100

Modeling of Heat Flow and Solidification During Atomization and Spray Deposition Processing

P. Shukla, N.S. Mishra, and S.N. Ojha

(Submitted 3 May 1997; in revised form 30 November 2002)

A mathematical model of the spray deposition process, based on heat flow analysis during solidification of droplets, as well as that of the spray deposit, is presented. The heat flow during cooling of droplets is analyzed in five distinct stages. A one-dimensional heat transfer model, using a finite difference method, is used to calculate the temperature of the deposit. The results indicate that the cooling rate of a wide size range of droplets of Al-4.5 Cu alloy in the spray varies from 10^3-10^5 °C s^{-1} in contrast to a slow cooling rate of 1-10 °C s^{-1} of the spray deposit. The spray enthalpy on the deposition surface increases linearly with the melt superheat. In contrast, the atomization gas pressure does not have a significant influence on the enthalpy of the spray in this process. The cooling rate of the deposits predicted from the model compares well with those obtained by the measurements.

Keywords cooling rate, droplets, modeling, solidification, spray deposition, undercooling

1. Introduction

In recent years, thermal spray deposition processes have created an exciting new opportunity in the synthesis of advanced materials. This process involves atomization of a molten material by high velocity gas jets into a spray of micron-sized droplets, which are subsequently propelled and deposited onto a substrate. Controlled maneuvering of the substrate results in the production of different shaped preform-like strips, billets, tubes, and rolls. Rapid solidification inherent in spray atomization, due to a high heat exchange rate at the droplet-gas interface and also on deposition surface, provides considerable chemical and microstructural homogeneity as well as refinement in the grain size of the deposit.

The microstructural evolution during spray deposition depends on the thermal state of the spray on the deposition surface. These, in turn, are controlled by the process variables used to atomize the melt and nozzle to substrate distance. Mathematical modeling provides a greater insight into understanding of the microstructural development during spray deposition. In the past, several investigations have been reported on the modeling of spray deposition processes.[1-5] It has been shown that a too large deposition distance generates a low volume fraction of the liquid on the deposition surface. This effect leads to poor bonding of particles and increased porosity of the deposit. Alternatively, a small deposition distance gives rise to increased liquid fraction that leads to gas entrapment and slow cooling rate of the spray deposit. This necessitates optimization of the process variables to achieve the desired microstructure during spray deposition. The process modeling helps in this direction. In the present investigation, droplets dynamics and their thermal state are predicted as a function of deposition distance. Subsequently, the cooling rate of the spray deposit is analyzed in the light of heat flux generated on the deposition surface and the heat extraction rate through the substrate.

P. Shukla and **S.N. Ojha,** Department of Metallurgical Engineering, Institute of Technology, Banaras Hindu University, Varanasi-221 005, India; and **N.S. Mishra**, National Institute of Foundry and Forge Technology, Ranchi-834002, India. Contact e-mail: ojha_bhu@yahoo.co.in.

2. Experimental Details

A spray nozzle with a throat area of 20.5 mm^2 and an exit to throat-area ratio of 3:1 was used for atomization of the melt. The axial gas velocity was measured by a Pitot tube (made indigenously in our laboratory) aligned below the nozzle exit. The Pitot tube was traversed axially downward, and readings were recorded at an interval of 5 mm. The static and stagnation ends of the Pitot tube were connected to a mercury manometer (also made in our laboratory) and readings were recorded at a reservoir pressure of 1.0 MPa. This provided data to calculate the gas velocity at a particular gas pressure and axial distance. The measured gas velocity showed an exponential decay with distance, with a velocity decay profile represented by the equation

$$V_g(z) = A + Be^{-\left(\frac{z-z_0}{C}\right)} \quad \text{(Eq 1)}$$

where the constants A, B, z_o, and C are 15.88, 376.06, 0.0326, and 0.080, respectively. The mass flow rate of the gas through the atomizer was measured by a rotameter (Eureka Instruments Co., Pune, India), which was calibrated for an inlet pressure of 1.25 MPa in a mass flow rate range of 0.61-6.1 kg min^{-1} of nitrogen.

Atomization of the melt was carried out using nitrogen gas at reservoir pressures of 0.8, 1.0, and 1.2 MPa to determine the effect of atomization pressure on particle size. The sieve analysis data provided the median particle diameters in the size range

of 60-70 μm, and these were used in the analysis of the heat flux calculations on the deposition surface. Two chromel-alumel thermocouples centered along the axis of the spray were inserted through a fine hole in the substrate. The hot junctions of the thermocouples were positioned at a height of 2 mm and 10 mm from the surface of the substrate. Temperature of the preform was measured at two deposition distances, i.e., 0.35 m and 0.45 m from the spray nozzle. The output of the thermocouples was recorded during and after deposition using a data acquisition system having a response time of 1.0 s.

3. Model Formulation

The heat transfer associated with spray deposition processing is considered in two distinct, but closely related, stages of atomization and deposition of droplets. A five-stage solidification regimen comprised of (1) cooling of the droplet in liquid state till nucleation, (2) recalescence of the undercooled droplet, (3) segregated solidification, (4) eutectic solidification, and (5) cooling in the solid state has been considered. A size-dependent undercooling of droplets based on volume separation of nucleants in the melt is used.[6,7] The computation is performed initially on droplets of specific sizes. Subsequently, the spray enthalpy is determined on the deposition surface. A one-dimensional heat transfer model, using a finite difference method, is used to calculate the temperature of the deposit by establishing a heat balance between the spray and the heat dissipated from the deposit.

3.1 Droplets Velocity and Their Thermal State

In spray atomization, the atomizing gas transfers a part of its kinetic energy to disintegrate the melt into droplets, and the remainder is used to accelerate the droplets towards the deposition surface. The relative velocity between the droplet and the gas determines the heat transfer coefficient. The equation for momentum provides the velocity of the droplets. Applying Newton's law of motion on the droplet yields a generalized equation of the form

$$m_d \frac{dV_d}{dt} = -\frac{1}{8}\rho_g A_d C_D |V_g - V_d|(V_g - V_d) + m_d g + \frac{\rho_g}{\rho_d} m_d g \qquad \text{(Eq 2)}$$

where V_g and V_d are the gas and droplet velocities, ρ_g and ρ_d are their densities respectively, m_d is the mass, and A_d is the surface area of the droplet. The first term on the right of Eq 2 denotes the drag force, the second denotes gravitational force, and the third denotes the buoyancy force acting on the droplet. The drag coefficient C_D arises due to flow separation around the droplet and is a function of the Reynolds number. The expression for C_D [8] for a wide range of Reynolds numbers varying from $0.1 < \mathrm{Re} < 4000$ is given by

$$C_D = 0.28 + \frac{6.0}{\mathrm{Re}^{0.5}} + \frac{21}{\mathrm{Re}} \qquad \text{(Eq 3)}$$

The expression for the axial velocity of the gas is taken from the measurements made in the present investigation.

A velocity dependent heat transfer coefficient is obtained by the well-known correlation of Szekely and Themelis.[9]

$$h_c = \frac{k_g}{d}(2.0 + 0.6\, Re^{0.5}\, Pr^{0.33}) \qquad \text{(Eq 4)}$$

where Re is the Reynolds number and Pr the Prandtl numbers; k_g is the thermal conductivity of the gas and d is the droplet diameter.

A generalized heat balance equation for a droplet during solidification is given by Levi and Mehrabian.[11]

$$\frac{dH_d}{dt} = C_{pd}\frac{dT_d}{dt} - \Delta H_d \frac{df_s}{dt} \qquad \text{(Eq 5)}$$

where C_{pd}, H_d, and f_s are the specific heat, specific enthalpy, and solid fraction of the droplet, respectively, and T_d is the instantaneous droplet temperature. C_{pd} and ΔH_d are given by

$$C_{pd} = C_L - (C_L - C_S) f_s \qquad \text{(Eq 6)}$$

$$\Delta H_d = \Delta H_f - (C_L - C_S)(T_L - T_S) \qquad \text{(Eq 7)}$$

where ΔH_f, C_L and C_s are the specific latent heat of fusion, specific heat of liquid, and solid phase, respectively; T_L and T_S are the liquidus and solidus temperatures of the alloy.

The left hand side in Eq 5 denotes the rate of change of enthalpy with time while the two terms in the right hand side, respectively, denote the change in sensible heat of the droplet and the latent heat released as a result of solidification. The droplets are subjected to undercooling prior to solidification. A model based on classic theory of heterogeneous nucleation and volume separation of nucleants among droplets size distribution is used to predict undercooling of droplets.[12] Assuming Newtonian cooling conditions, the thermal history of an undercooled droplet is obtained by equating the rate of change of enthalpy with time to the heat convected at the droplet-gas interface as represented by

$$\frac{dH_d}{dt}\rho_d \overline{V}_d = -A_d h_c (T_d - T_g) \qquad \text{(Eq 8)}$$

Here $\overline{V}_d$ denotes the volume of a droplet. Equation 8 is applicable to all the five stages of cooling and solidification with relevant modifications. For the cooling of a semisolid droplet, both the latent heat of fusion and the sensible heat have to be taken into consideration. Substituting Eq 8 into Eq 6 and 7 gives a thermal energy balance for a droplet of given size as

$$C_{pd}\frac{dT_d}{dt} = \Delta H_d \frac{df_s}{dt} - \frac{6h_c}{\rho_d d}(T_d - T_g) \qquad \text{(Eq 9)}$$

Different solidification front velocity profiles have been used to relate the fraction solidified including linear and exponential laws for planar growth at small and large undercooling.[10] In the present case, a linear growth profile has been used with the assumption that nucleation occurs at the droplet surface with the solidification interface moving in diametrically opposite direction. The fraction solidified is given by Levi and Mehrabian[11]

$$f_s = \frac{3}{2}\left(\frac{x}{d}\right) - \frac{1}{2}\left(\frac{x}{d}\right)^3 \qquad \text{(Eq 10)}$$

where x is the distance solidified along the radial growth direction. The crystal growth velocity for a low degree of undercooling[11] is approximated as

$$\frac{dx}{dt} = k_i(T_i - T_d) \quad \text{(Eq 11)}$$

where k_i is the solid-liquid interface mobility factor taken as 0.02 m s^{-1} K^{-1}. It is important to note that Eq 11 is applicable for small-to-moderate undercooling of the melt. The growth velocity for highly undercooled melt shows a power law relationship with melt undercooling.[13] However, due to lack of information regarding the value of k_i for highly undercooled melt, Eq 11 has been invariably applied for a small-to-moderate degree of undercooling of the melt. Eq 1-11 are solved to determine the temperature of the droplets during their five distinct stages of solidification. The thermo-physical properties of Al-4.5 wt.%Cu have been taken from Kurz and Fisher[14] and that of N_2 gas from Holman.[15]

3.2 Heat Flow During Spray Deposition

The modeling of heat transfer during the deposition stage follows from the knowledge of the heat transfer and solidification behavior of droplets in the spray. The thermal condition of the spray at the time of impingement is assumed to represent the thermal condition of the entire spray. On the basis of this assumption and with the mass flow rate of the melt known, the incoming spray enthalpy is calculated.

The equation governing the heat transfer in the preform using an enthalpy formulation is given by Holman [15]

$$\rho\frac{\partial H}{\partial t} = k\frac{\partial}{\partial y}\left(\frac{\partial T}{\partial y}\right) \quad \text{(Eq 12)}$$

where ρ is the density of the deposited material, H is the enthalpy, T is the temperature, t is time, y is the distance in the growth direction, and k is the average thermal conductivity of the deposited material. The average thermal conductivity is the mean of thermal conductivity of liquid and solid melts. Enthalpy has been used in the above formulation to take into account the change in heat content as a result of solidification. At the bottom surface of the deposit, a heat flux balance yields

$$k\frac{\partial T}{\partial y} = h_{bot}[T - T_{sub}] \quad \text{(Eq 13)}$$

At the top surface of the growing deposit, the heat balance is given by

$$k\frac{\partial T}{\partial y} = \overline{H}\dot{Y} + h_{top}[T - T_{gas}] \quad \text{(Eq 14)}$$

In Eq 12-14, $\overline{H}$ is the net enthalpy input at the top surface of the preform and is equal to the difference between the enthalpies of the incoming spray and that of the topmost layer of the deposit, and $\dot{Y}$ is the deposition rate per unit area. In the present investigation, the value of h_{bot} of 1100 W m^{-2} K^{-1} has been used during the deposition stage. The convective heat transfer coefficient value of 200 W m^{-2} K^{-1} during the deposition stage, and 100 W m^{-2} K^{-1} during natural cooling in the post-deposition stage, has been used. These values are commensurate with those reported by other investigators.[7] The solution of Eq 13 requires the temperature at a few initial grid points to start the computation. We assign arbitrary values of temperature to three grid points. These grid points are the bottom-most point and the next two points above it.

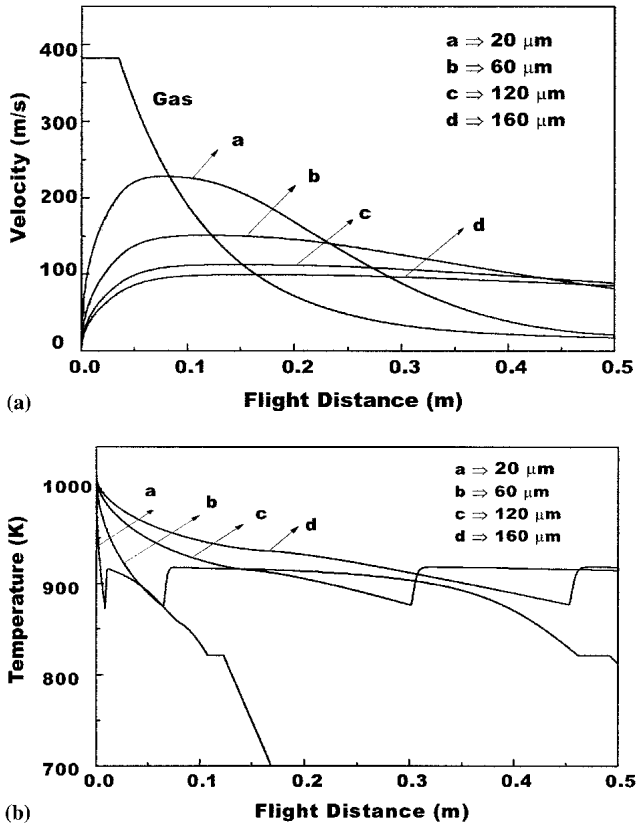

Fig. 1 Variation in **(a)** velocity profile and **(b)** temperature as a function of flight distance for a large-size range of droplets

4. Results and Discussion

4.1 Velocity and Temperature of Droplets

Figure1(a) shows the variation in velocity of different-sized droplets as a function of flight distance. Superimposed on the graph is the velocity profile of the atomizing gas. The gas exit velocity is 384 m s^{-1}, attained at an atomizing pressure of 1.0 MPa. A small-size droplet is observed to accelerate to a maximum velocity at a relatively small flight distance compared with that of a large-size droplet. A comparison of the velocity profiles of a wide size range of droplets in the spray shows that a 20 μm droplet is observed to attain a maximum velocity of 230 m s^{-1} in less than 0.1 m compared with a maximum velocity of 100 m s^{-1} of a 160 μm size droplet. Other intermediate-size droplets show a similar behavior. In addition, small-size droplets are observed to rapidly decelerate at smaller flight distances compared with large-size droplets. The bigger droplets are slowly decelerated,

Table 1 Effect of Droplet Size on Undercooling, Initial Growth Rate, and Fraction Solidified During Recalescence

d, μm	ΔT, °C	T_R, °C	V_i, ms^{-1}	f_R, %
20	177	644	3.5	53
40	112	645	2.2	33
80	61	645	1.2	20
160	11	645	0.2	5

Table 2 Spray Characteristics at Two Different Deposition Distances

Deposition Distance, m	Spray Temperature, °C	Solid Fraction, f_S	Spray Enthalpy, kJ kg^{-1}
0.35	632	0.62	212
0.45	600	0.84	104

as they possess greater inertia, while the smaller ones experience a sharp decrease in their velocities. The temperature-time cooling curves of different-size droplets subjected to the same undercooling are presented in Fig.1(b). It is interesting to note that a small-size droplet of 20 μm experiences five distinct stages of cooling, while a large-size droplet reaches the deposition surface before its solidification. The results also indicate that a 20 μm size droplet is subjected to a cooling rate of the order of 10^5 Ks^{-1} in contrast to a cooling rate of 10^3 Ks^{-1} of a 160 μm size droplet in the spray. However, the undercooling of a droplet depends on its size. This effect is difficult to assess in the melt atomization processes. A statistical analysis of the volume separation of nucleants among droplets' size distribution and classic nucleation theory have been used to obtain the nucleation temperature of droplets.[12] This behavior of droplet solidification has been used to analyze an overall enthalpy of the spray on the deposition surface. The undercooling and solid fraction generated during different solidification regimes of a wide size-range of droplets in the spray is shown in Table 1. The results indicate that the recalescence arrest temperature of undercooled droplets invariably reaches to liquidus temperature of the alloy. The fraction solidified during recalescence stage (f_R) of a small-size droplet of 20 μm is more than 0.50 that decreases to 0.05 for a droplet of 160 μm size. Similarly, an initial interface velocity (V_i) of a 20 μm droplet is 3.5 ms^{-1} against that of 1.2 ms^{-1} for an 80 μm droplet. Other intermediate-size droplets exhibit a similar variation in the interface velocity and the fraction solidified during the recalescence stage. This mode of solidification of undercooled droplets contributes to development of the metastable microstructure in the spray deposit. However, further solidification of large-size droplets occurs by the mode of solute segregation.

The temperature profile during solidification of two widely different-size droplets undercooled by 45 and 175 K is shown in Fig. 2(a). The five distinct stages of cooling and solidification are clearly observed for the case of a 20 μm droplet. Considering a constant undercooling of 45 °C for a 160 μm droplet, its nucleation process is delayed to a longer flight distance compared with the nucleation occurring at a small flight distance if size-dependent undercooling of 11 °C is considered. In contrast, when the same constant undercooling is assumed for a 20 μm size droplet, the nucleation event is observed at a smaller flight

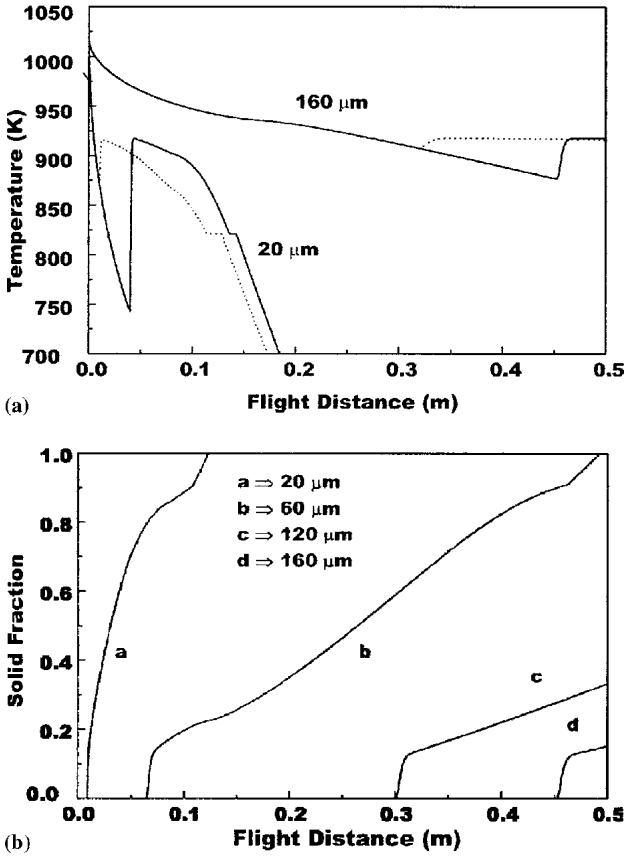

Fig. 2 Variation in **(a)** temperature profile of two different size droplets and **(b)** solid fraction of a wide size range of droplets with flight distance

distance compared with that based on analysis of its size-dependent undercooling. This result indicates that an assumption of the same constant undercooling overestimates the degree of undercooling of a large-size droplet. This effect of droplet undercooling has a strong influence on its predicted solid fraction on the deposition surface. The solid fraction generated in the above droplet sizes is shown in Fig. 2(b). A larger undercooling increases the solid fraction formed during recalescence of a 20 μm droplet from 0.15 (ΔT = 45 °C) to 0.5 (ΔT = 175 °C). The solid fraction generated during segregated solidification increases at a lower undercooling of a droplet. This marked variation in the fraction of solid formed during different stages of solidification due to a different degree of undercooling will greatly influence the microstructure of the droplet and subsequently that of the preform.

4.2 Spray Enthalpy

The spray characteristics represent the aggregate effect of droplets comprising the spray under different atomizing conditions. The effect of gas pressure and melt superheat on the spray enthalpy at various deposition distances is presented in Fig. 3(a) and (b). It is observed that the spray enthalpy decreases with an increase in the deposition distance. A large flight time at greater deposition distances facilitates heat removal, and consequently, a larger fraction of solid is formed. An increase in atomization pressure results in higher gas exit velocity and resultant decrease

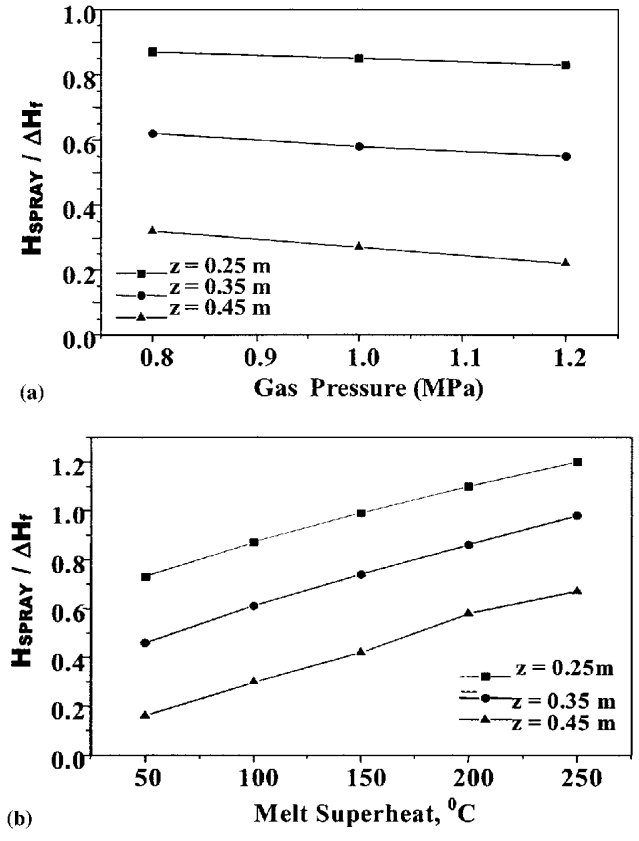

Fig. 3 Effect of **(a)** atomization gas pressure and **(b)** melt superheat on spray enthalpy at three different deposition distances

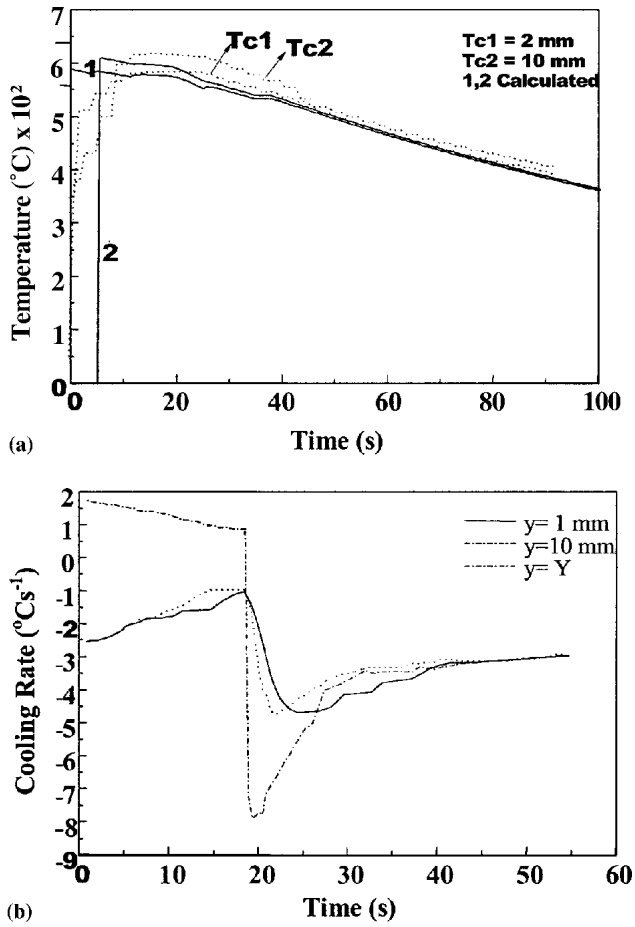

Fig. 4 A comparison in **(a)** calculated and measured temperature profile and **(b)** cooling rate of the spray deposit at a distance of 2 and 10 mm from the substrate surface

in size of the droplets. A higher gas velocity invariably leads to a reduction in flight time, while smaller droplets have higher cooling rates. A reduction in flight time leads to a smaller fraction solidified, while increased cooling rate has the opposite effect. Hence, the fraction solidified is determined by the relative magnitude of these effects. It is observed that a higher fraction of the spray solidifies as the deposition distance is increased. The results of process variables and powder characterization obtained during the atomization experiments along with the modeling of droplet dynamics and heat transfer during flight enable us to determine the spray characteristics at various deposition distances. The results for the two deposition distances used at an atomization gas pressure of 1.0 MPa are presented in Table 2.

In addition, as the melt superheat increases, the solid fraction at a particular deposition distance decreases. The spray solid fraction decreases from 0.60 to about 0.40 as the melt superheat is increased from 100-200 °C at a deposition distance of 0.35 m. This change is significant when compared with the effect of atomization gas pressure on incoming spray enthalpy (Fig. 3) where there is a marginal change in spray enthalpy owing to changing gas pressure. It is inferred that at a particular deposition distance, melt superheat has a greater influence on the solid fraction than gas pressure. This is of practical importance during spray deposition. Since the shape and microstructure of the preform depends upon the liquid content impinging on the top surface of the spray deposit, a judicious choice of melt superheat and the atomization gas pressure can be used to produce optimum shape and the desired microstructure of the spray deposit.

4.3 Cooling Rate of the Spray Deposit

A comparison of the measured and calculated temperature profiles at a nozzle to substrate distance of 0.35 m is presented in Fig. 4(a). The thermocouples Tc1 and Tc2 record the temperature in the preform at 2.0 mm and 10.0 mm, respectively, from the substrate surface. The recorded temperature shows a sharp initial peak due to droplets impinging on the tip of the thermocouples. Tc1 attains a stable profile earlier than Tc2 because it is embedded earlier in the growing preform. A cap of frozen metal is formed at the tip of Tc2 due to the spray depositing over the ceramic sheath encasing the thermocouple wire. Hence, the temperature recorded by Tc2 shows fluctuations until it is fully embedded after 6 s from the start of the deposition process. Tc1 records temperature close to 580 ^{o}C, while Tc2 records a peak temperature of 615 ^{o}C during the deposition period of 19 s. The termination of the deposition is manifested by a marked change in the slopes of the two curves after a deposition period of 19 s. In the later stages, after the temperature has fallen below the solidus temperature (T_S) of the alloy, it is observed that the rate of drop of the temperature diminishes. This observation is attributed to the fact that after solidification, the preform lifts up from the substrate surface due to shrinkage stress in the preform. The loss of contact between the bottom of the preform and the substrate

results in a decrease in the rate of heat loss through conduction from the bottom of the preform. It is observed that Tc2 records a stable temperature profile only after a deposition time of about 2 s. The measured temperature drop after the end of deposition does not exhibit an exponential decay profile as reported by other investigators.[5] The difference in this behavior could arise due to the water-cooled copper substrate used in their investigation compared with a steel substrate used in the present investigation. A water-cooled copper substrate would ensure more effective heat transfer through conduction from the bottom of the preform and consequently a faster drop in temperature.

On the basis of the calculated temperature profiles, the cooling rate at a distance of 2 mm, 10 mm, and that of the instantaneous top deposition surface during spray deposition of the preform in both the experiments are calculated and shown in Fig. 4(b). It is worthwhile to note that at a distance of 2 mm from the bottom of the deposit in Experiment 1, an initial cooling rate of 2.5 K s^{-1} is experienced. The cooling rate gradually decreases with an increase in the thickness of the deposit during subsequent deposition process. This effect arises primarily due to the low heat extraction rate from the mild steel substrate with no cooling arrangement. The substrate temperature rises as the deposit builds up, thereby reducing the heat transfer by conduction through the substrate. The cooling rate drastically increases when the deposition process ceases. The maximum cooling rate reached at this location is only 5 °C s^{-1}, which further decreases to 3 °C s^{-1} during the post solidification stage. The results show that a maximum cooling rate of 8 °C s^{-1} is reached after 19 s, i.e., at the end of the deposition process. The cooling rate then decreases to a constant value of 3 °C s^{-1}. The sharp drop in the cooling rate profile of the instantaneous top surface as compared with that of the bottom surface is due to the sudden removal of incoming heat flux at the top surface, while the bottom still continues to receive heat from the overlying preform material. The cooling rate profile at 10 mm from the bottom is also shown on the same graph. It is noted that the cooling rate is lesser than at the bottom. This is due to its proximity to the continuous heat source at the top. The nominal difference in the cooling rates experienced by the different surfaces gives an insight into understanding the evolution of microstructure in spray deposited materials. In summary, the results of the present investigations indicate that the cooling rate of the deposit is many orders of magnitude lower than those of the atomized droplets.

5. Conclusions

The cooling rate of a droplet in the spray depends on its size and relative velocity with the gas stream. A wide size-range of droplets in the spray varying from 20-200 μm size are subjected to a cooling rate of 10^3-10^5 °C s^{-1} with the highest cooling rate of the small-size droplets. In contrast, the cooling rate of the spray deposits vary from 1-10 °C s^{-1}. A small-size droplet of 20 μm is subjected to a large undercooling and its maximum solid fraction is generated during the recalescence stage. The solidification of large-size droplets occurs by the mode of segregated solidification. The spray enthalpy on the deposition surface increases linearly with the melt superheat. An increase in melt superheat from 50-200 °C results in an increase in the spray enthalpy by 2.5 times on a deposition distance of 0.45 m. However, the spray enthalpy is not significantly influenced by varying the gas pressure from 0.8-1.2 MPa. The cooling rate of the spray deposit predicted from the model compares well with those obtained by experimental measurements.

References

1. E.J. Lavernia, E. Gutierrez-Miravete, J. Szekely, and N.J. Grant: "A Mathematical Model of the Liquid Dynamic Compaction Process. Part 1: Heat Flow in Gas Atomization," *Int. J. Rapid Solidification*, 1988, *4*(1/2), pp. 89-124.
2. P. .Mathur, S. Annavarapu, D. Apelian, and A. Lawley: "Spray Casting: An Integral Model for Process Understanding and Control," *Mater. Sci. Eng.*, 1991, *A142*, pp. 261-76.
3. P.S. Grant, B.Cantor, and L.Katgerman: "Modeling of Droplet Dynamics and Thermal Histories During Spray Forming: 1. Individual Droplet Behavior," *Acta Metall. Mater.*, 1993, *41*, pp. 3097-3108.
4. E. Lee and S. Ahn: "Solidification Progress and Heat Transfer Analysis of Gas Atomized Alloy Droplets During Spray Forming," *Acta. Metall. Mater.*, 1994, *42*, pp. 3231-43.
5. B.P. Bewlay and B. Cantor: "The Relationship Between Thermal History and Microstructure in Spray Deposited Tin-Lead Alloys," *J. Mater. Res.*, 1991, *6*(7), pp. 1433-54.
6. A.J. Drehman and D. Turnbull: "Solidification Behavior of Undercooled $Pd_{83}Si_{17}$ and $Pd_{82}Si_{18}$ Liquid Droplets," *Scripta Metall.*, 1981, *15*, pp. 543-48.
7. E.J. Lavernia and Y.Wu: *Spray Atomization and Deposition*, 1st ed., John Wiley and Sons, UK, 1996, p. 106.
8. H. Kurten: *Bubbles, Drops and Particles*, Academic Press, NY, 1978, pp. 42-87.
9. J. Szekely and N. Themelis: *Rate Phenomena in Process Metallurgy*, John Wiley & Sons, New York, NY, 1971, pp.170-207.
10. C.G. Levi and R. Mehrabian: "Heat Flow in Atomized Metal Droplets," *Met. Trans.B*, 1980, *11B*, pp. 21-27.
11. C. G.Levi and R.Mehrabian: "Heat Flow During Rapid Solidification of Undercooled Metal Droplets," *Metall. Trans.*, 1982, 13A, pp. 221-34.
12. P. Shukla, R.K. Mandal, and S.N. Ojha: "Non-Equilibrium Solidification of Undercooled Droplets During Atomization Process," *Bull. Mater. Sci.*, 2001, *24(5)*, pp. 547-54.
13. D.M. Herlach: "Non-Equilibrium Solidification of Undercooled Metallic Droplets," *Mater. Sci. Eng.*, 1994, *R12*, pp. 177-272.
14. W. Kurz and D.J. Fisher: *Fundamentals of Solidification*, Trans Tech Publication, Aedermannsdorf, Switzerland, 1989, p. 241.
15. J.P. Holman: *Heat Transfer*, McGraw Hill Book Company, NY, 1989, p. 27-178.